Sloshing Dynamics Induced Angular Momentum Fluctuations Driven by Jitter Accelerations Associated with Slew Motion in Microgravity

By

R. J. HUNG, Y. T. LONG and H. L. PAN

Reprinted from

TRANSACTIONS OF THE JAPAN SOCIETY FOR
AERONAUTICAL AND SPACE SCIENCES

VOL. 37, NO. 117, 1994

Sloshing Dynamics Induced Angular Momentum Fluctuations Driven by Jitter Accelerations Associated with Slew Motion in Microgravity*

By R. J. HUNG,** Y. T. LONG** and H. L. PAN**

Key Words: Sloshing Dynamics, Microgravity, Spacecraft Slew Motion, Superfluid Helium, Gravity Jitter

Abstract

The mathematical formulation of orbital spacecraft sloshing dynamics for partially filled liquid of cryogenic superfluid helium II in dewar container driven by the gravity jitter acceleration associated with slew motion are studied. The Advanced X-Ray Astrophysics Facility-Spectroscopy (AXAF-S) spacecraft is chosen as a practical example in this study. Explicit mathematical expressions to manage orbital gravity jitter acceleration associated with slew motion which is acting on the spacecraft fluid systems are derived. The numerical computation of sloshing dynamics is based on the non-inertia frame spacecraft bound coordinate, and solve time-dependent, three-dimensional formulations of partial differential equations subject to initial and boundary conditions. This study discloses capillary effect of sloshing dynamics governed liquid-vapor interface fluctuations, angular momentum and moment fluctuations of fluid system, driven by the gravity jitter acceleration associated with slow motion which affects the stability of the orbital spacecraft fluid system in a microgravity environment.

1. Introduction

For the purpose to carry out scientific experiments, some experimental spacecraft use cryogenic cooling for observation instrumentation and telescope, superconducting sensors for gyro read-out and maintain very low temperature near absolute zero for mechanical stability. The approaches to both cooling and control involve the use of superfluid liquid helium II. To give examples, both Gravity Probe-B (GP-B) and Advanced X-Ray Astrophysics Facility-Spectroscopy (AXAF-S) spacecrafts adopt the cooling and boil-off from the cryogenic liquid helium dewar as a cryogen and propellant to maintain the cooling of instrumentations, attitude control and drag-free operation of the spacecraft. The potential problems for cryogenic liquid in dewar container could be due to *asymmetry* in the liquid helium and vapor distribution and to perturbations in the liquid-vapor-solid interface caused by slosh wave excitation driven by pointing control, machinery vibration, etc.

* Received November 26th, 1993.

** Department of Mechanical and Aerospace Engineering, College of Engineering, The University of Alabama in Huntsville, Huntsville, Alabama 35899, U.S.A.

For the cases of both the GP-B and the AXAF-S spacecrafts, cryogenic liquid helium II, at a temperature of 1.3°K, is used as the propellant. With its superfluid behavior, there is no temperature gradients in the liquid helium. In the absence of temperature gradient along the surface which drive Marangoni convection, the equilibrium shape of the free surface is governed by a balance of capillary, centrifugal and gravitational forces. Determination of liquid-vapor interface profiles based on computational experiments can uncover details of the flow which can not be easily visualized or measured experimentally in a microgravity environment.

The instability of the liquid-vapor interface surface can be induced by the presence of longitudinal and lateral accelerations. Slosh waves are, thus, excited which produces high and low frequency oscillations in the liquid propellant. The sources of the residual accelerations range from the effects of the Earth's gravity gradient and jitter accelerations which include, atmospheric drag on the spacecraft, vibration of compressor, spacecraft attitude motions arising from machinery vibrations, thruster firings, spacecraft slew motion, pointing control of spacecraft, crew motion, etc. Recent study[1] suggest that the high frequency accelerations may be unimportant in comparison to the residual motions caused by low frequency accelerations.

Time-dependent dynamical behavior of partially-filled rotating fluids in reduced gravity environments was simulated by numerically solving the Navier Stokes equations subject to the initial and the boundary conditions.[2-5] At the interface between the liquid and the gaseous fluids, both the kinematic surface boundary condition, and the interface stress conditions for components tangential and normal to the interface, were applied.[6-10] The initial conditions were adopted from the steady-state formulations developed by Hung et al.[11-13] Some of the steady-state formulations of interface shapes were compared with the available experiments carried out by Leslie[14] in a free-falling aircraft (KC-135). The experiments carried out by Mason et al.[15] showed that the classical fluid mechanics theory is applicable for cryogenic liquid helium in large containers.

In the spacecraft orbit around the Earth, the direction of azimuth angle of the Earth toward the location of the spacecraft mass center varies from 0° along the rolling axis of spacecraft to various directions in which three dimensional calculation shall be adopted.

As the spacecraft moves along the orbit, any fluid capable of motion relative to the spacecraft is subject to the acceleration that arises from the gravity gradients of the Earth.[16-18] The interaction between the particle mass of fluid and the spacecraft mass due to gravity gradient accelerations[17] are capable for the excitation of slosh waves and disturb the fluid system which induces the angular momentum and its moment fluctuations. In the meanwhile, the sources of residual acceleration of gravity jitter range from atmospheric drag on the spacecraft, background gravity, spacecraft attitude motions arising from machinery vibrations, pointing control of spacecraft, spacecraft slew motion, thruster firings, crew motion, etc., are also capable for the excitation of slosh waves on the fluid containers.

It is critically important to understand the physical and dynamical behavior of liquid helium II in a rotating cylinder to effectively promote space-oriented missions of cryogenic sloshing dynamics in microgravity.

At temperatures close to absolute zero, quantum effects begin to be of importance

in the properties of fluids. At a temperature of 2.17°K, liquid helium has a λ-point (a second-order phase transition); at temperatures below this point, liquid helium (helium II) has a number of remarkable properties, the most important of which is superfluidity. This is the property of being able to flow without viscosity in narrow capillaries or gaps.

The basis of the dynamics of helium II is the following fundamental result of microscopic theory. At temperatures other than zero, helium II behaves as if it were a mixture of two different liquids. One of these is a superfluid and moves with zero viscosity along a solid surface. The other is a normal viscous fluid. It is of great importance that no friction occurs between these two parts of the liquid in their relative motion, i.e., no momentum is transferred from one to the other.

It should be emphasized that regarding the liquid as a mixture of normal and superfluid parts is no more than a convenient description of the phenomena which occur in a fluid where quantum effects are important. One of these motions is normal and has the same properties as the motion of an ordinary viscous fluid, but the other is the motion of a superfluid. The two motions occur without any transfer of momentum from one to another for velocities below a critical velocity.[19,20] For two components of normal and superfluid velocities above a critical velocity, the two fluids are nearly coupled.[19,20]

If fluid flow can separate helium II into the regions of the superfluid and the normal fluid, two temperatures zones are immediately created. A very low temperature zone is located at the zone of very high density concentration of the superfluid, while a high temperature (below 2.17°K) zone is located at the zone of very high density concentration of the normal fluid at the other end. The existence of a sharp temperature gradient at the interface between the superfluid and the normal fluid results in the creation of a great difference in chemical potential, which, in turn, induces a great reverse pressure gradient, creating the environment of isothermal fluid distribution everywhere throughout the cylinder and homogenous distribution of superfluid density concentration. This illustration of the possible separation of superfluid from normal fluid of helium II means that there is in reality, no way for anyone to achieve the separation of the superfluid from the normal fluid of helium II. A key parameter of critical velocity to distinguish one fluid from two-fluid models is a function of fluid temperature and container size.[19,20] In other words, in considering the dynamical behavior of helium II in a large rotating cylinder, a mixture of the superfluid and the normal fluid without separation of the two fluids is accounted for in the model computation. Density concentration of superfluid is a function of temperature, which is also true for the surface tension and viscous coefficient for helium II.[21-24] In fact, the experiments carried out by Mason et al.[15] showed that the classical fluid mechanics theory is applicable for cryogenic liquid helium in a large container. In this study, the theory of viscous Newtonian fluids is employed with modification of transport coefficients adjusted by normal and superfluid density concentration which is a function of temperature.

2. Functions of Scientific Observation and Spacecraft Motions

Various scientific satellites operate on different orbits depending upon the scientific missions. We are particularly interested in the spacecraft operating with spinning and/or slew motions when it is operating around the Earth. The AXAF-S spacecraft is a sun

synchronous Earth satellite orbiting at 650 km altitude directly over the poles and also operating with spinning and/or slew motions.

The AXAF-S with its sister spacecraft AXAF-I (I for imaging) are two spacecrafts restructured from the original AXAF design to carry out astrophysical observation. Equipped with the (microcalorimeter) X-Ray Spectrometer (XRS), AXAF-S provides high-throughput, high-resolution, non-dispersive spectroscopy at the higher AXAF X-ray energies—including the astrophysically important iron-K spectral region (above 6.4 keV)—and also permits some spatially resolved high-resolution spectroscopy. AXAF-S comprises a foil-mirror (or possibly, a replication-optic) telescope (4.7-m focal length), with XRS in the focal plane. With the baseline optical system, the AXAF-S provides important, unique capabilities for high-throughput, high resolution (above 1 keV) spectroscopy of extended and point sources and for some spatially resolved high-resolution spectroscopy.

To comprise these functions of scientific observation, AXAF-S equipped with foil-mirror telescope and XRS in the focal plane is capable to observe point and extended sources of active galactic nuclei, clusters of galaxies, supernova remnants, X-ray binaries, stellar flares, active regions of corona, etc., through spacecraft slew motion of pointing control. In other words, spacecraft slew motion without spinning with rotating axis is required for AXAF-S to perform its scientific mission.

3. Basic Characteristics of Gravity Jitter Acceleration Associated With Slew Motion

Let us consider the case of the AXAF-S spacecraft, which is the Earth satellite orbiting at 650 km altitude directly over the poles, the orbit period, τ_o can be computed from following expression:

$$\tau_o = 2\pi \frac{R_c^{3/2}}{R_E g_0^{1/2}} \quad \ldots\ldots(3\text{-}1)$$

where R_E denotes the radius of Earth ($=6373$ km); R_c, the radius of the circular orbit ($=R_E+h=7023$ km); h, orbit altitude ($=650$ km); and g_0, Earth gravity acceleration ($=9.81$ m/s^2). For the case of the AXAF-S spacecraft, the orbit period $\tau_o=97.6$ min, and orbit rate $n=2\pi/\tau_o=1.07\times10^{-3}$ rad/s.

As the spacecraft is orbiting around the Earth, the azimuth angle of the Earth, ψ_E, toward the location of the spacecraft mass center varies with respect to time. At time $t=0$, the rolling axis of the spacecraft is aligned with the radial direction of the Earth's center to the spacecraft mass center. Assuming the spacecraft rolling axis is linearly turning around 0° to 360° in the orbit period, τ_o, of the spacecraft when the spacecraft is orbiting around the Earth. Without the spacecraft slew motion, the azimuth angle (ψ_{Eo}) can be defined as

$$\psi_{Eo} = \frac{2\pi}{\tau_o} t \quad \ldots\ldots(3\text{-}2)$$

where τ_o is the spacecraft orbit period [defined in Eq. (3-1)]; and t is the time measured from the instant when the direction of the spacecraft rolling axis is aligned with the radial direction of the spacecraft mass center to the center of the Earth.

3.1. Slew motion of spacecraft For the purpose to carry out wide-range observations, some scientific spacecraft requires slew motion with respect to the mass center of the spacecraft. This is particularly true for the case of the AXAF-S spacecraft. For the case of the spacecraft slew motion, azimuth angle, shown in Eq. (3-2), shall be modified through the coordinate transformation of slew motion when the spacecraft is orbiting around the Earth.

It is assumed that the slew motion starts at the mass center of the spacecraft. Let us choose cartesian coordinate (x'', y'', z'') with z''-axis along the axis of the dewar container (see Fig. 1). At time $t=0$, the radial vector $\hat{r}_c$ from the center of the spacecraft to the center of the Earth lies on the x''–z'' plane of the cartesian coordinate chosen (see Fig. 1). The azimuth angle ψ_E is defined as the angle between the radial vector $\hat{r}_c$ and the z''-axis. Rotation matrices for spinning and/or slew motions along the x''-, y''- and z''-axes can be expressed as

$$\begin{bmatrix} 1 & 0 & 0 \\ 0 & \cos\omega_x t & \sin\omega_x t \\ 0 & -\sin\omega_x t & \cos\omega_x t \end{bmatrix}, \begin{bmatrix} \cos\omega_y t & 0 & -\sin\omega_y t \\ 0 & 1 & 0 \\ \sin\omega_y t & 0 & \cos\omega_y t \end{bmatrix}, \begin{bmatrix} \cos\omega_z t & \sin\omega_z t & 0 \\ -\sin\omega_z t & \cos\omega_z t & 0 \\ 0 & 0 & 1 \end{bmatrix}$$

respectively. Here, ω_x, ω_y and ω_z denote angular velocity of slew and/or spinning motions along the x''-, y''- and z''-axes, respectively. Radial vector $\hat{r}_c$ in cartesian coordinate without slew and spinning motion is (see Fig. 1)

$$\hat{r}_{co} = [\sin\psi_{Eo}, 0, -\cos\psi_{Eo}] \quad \ldots.(3\text{-}3)$$

With an execution of spinning motion along the z''-axis only, radial vector $\hat{r}_c$

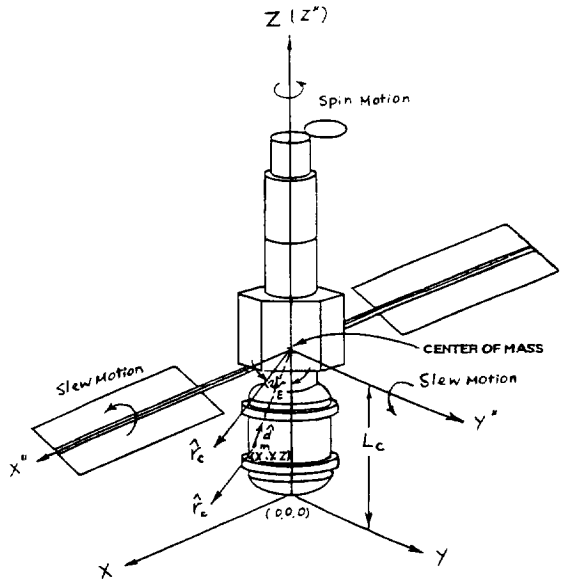

Fig. 1. AXAF-S spacecraft coordinate systems with azimuth angle ψ_E from spacecraft mass center to the center of the Earth. Coordinate (x'', y'', z'') for slew motion and coordinate (x, y, z) for fluid mechanics computation.

becomes (see Fig. 1)

$$\hat{r}_{c-z}=\begin{bmatrix} \cos\omega_z t & \sin\omega_z t & 0 \\ -\sin\omega_z t & \cos\omega_z t & 0 \\ 0 & 0 & 1 \end{bmatrix}\begin{bmatrix} \sin\psi_{Eo} \\ 0 \\ -\cos\psi_{Eo} \end{bmatrix}$$

$$=[\sin\psi_{Eo}\cos\omega_z t,\ -\sin\psi_{Eo}\sin\omega_z t,\ -\cos\psi_{Eo}] \quad \ldots.(3\text{-}4)$$

With an execution of slew motion along the y''-axis only, radial vector $\hat{r}_c$ becomes (see Fig. 1)

$$\hat{r}_{c-y}=\begin{bmatrix} \cos\omega_y t & 0 & -\sin\omega_y t \\ 0 & 1 & 0 \\ \sin\omega_y t & 0 & \cos\omega_y t \end{bmatrix}\begin{bmatrix} \sin\psi_{Eo} \\ 0 \\ -\cos\psi_{Eo} \end{bmatrix}$$

$$=[\sin(\psi_{Eo}+\omega_y t),\ 0,\ -\cos(\psi_{Eo}+\omega_y t)] \quad \ldots.(3\text{-}5)$$

With an operation of slew motion along the x''-axis only, radial vector $\hat{r}_c$ becomes (see Fig. 1)

$$\hat{r}_{c-x}=\begin{bmatrix} 1 & 0 & 0 \\ 0 & \cos\omega_x t & \sin\omega_x t \\ 0 & -\sin\omega_x t & \cos\omega_x t \end{bmatrix}\begin{bmatrix} \sin\psi_{Eo} \\ 0 \\ -\cos\psi_{Eo} \end{bmatrix}$$

$$=[\sin\psi_{Eo},\ -\cos\psi_{Eo}\sin\omega_x t,\ -\cos\psi_{Eo}\cos\omega_x t] \quad \ldots.(3\text{-}6)$$

In other words, radial vector $\hat{r}_c$ will be modified from the mathematical expression shown in Eqs. (3-3) to (3-4), (3-5) and (3-6) for the slew and/or spinning motions along the z''-, y''- and x''-axes alone, respectively. In particular, for the case of slew motion along the y''-axis, comparison between Eqs. (3-3) and (3-5), it shows that the azimuth angle will be modified as

$$\psi_E=\psi_{Eo}+\omega_y t \quad \ldots.(3\text{-}7)$$

For the successive operations of the spacecraft from spinning motion along the z''-axis, then slew motion along the y''-axis, and then slew motion along the x''-axis, radial vector $\hat{r}_c$ results

$$\hat{r}_{c-z,y,x}=\begin{bmatrix} 1 & 0 & 1 \\ 0 & \cos\omega_x t & \sin\omega_x t \\ 0 & -\sin\omega_x t & \cos\omega_x t \end{bmatrix}\begin{bmatrix} \cos\omega_y t & 0 & -\sin\omega_y t \\ 0 & 1 & 0 \\ \sin\omega_y t & 0 & \cos\omega_y t \end{bmatrix}$$

$$\cdot\begin{bmatrix} \cos\omega_z t & \sin\omega_z t & 0 \\ -\sin\omega_z t & \cos\omega_z t & 0 \\ 0 & 0 & 1 \end{bmatrix}\begin{bmatrix} \sin\psi_{Eo} \\ 0 \\ -\cos\psi_{Eo} \end{bmatrix} \quad \ldots.(3\text{-}8)$$

In addition to the modification of the azimuth angle made by the spacecraft slew motion, accelerations are also induced to activate on the fluid mass in the dewar container. Accelerations acting on the fluid particle in the dewar induced by the slew motion of the spacecraft with the coordinate fixed at the spacecraft center of the mass is as follows (see Fig. 1):

$$\ddot{\vec{R}}_p = \dot{\vec{\omega}} \times (\vec{\omega} \times \vec{R}_p) + \vec{\alpha} \times \vec{R}_p + 2\vec{\omega} \times \vec{v} \quad \ldots\ldots(3\text{-}9)$$

where $\vec{R}_p$ denotes the position vector of the fluid particle in the dewar container relative to the body frame of the spacecraft; $\vec{\omega}$, angular velocity of the spacecraft body frame; $\vec{\alpha}$, angular acceleration of the spacecraft body frame; and $\vec{v}$, velocity of the fluid particle relative to the spacecraft body frame.

As we indicated earlier, let us assume that the slew motion starts at the spacecraft mass center, so is cartesian coordinate (x'', y'', z'') chosen with origin located at the spacecraft mass center. Let us also assume that x''–z'' plane intersects the center of Earth and the spacecraft mass center. In other words, azimuth angle of Earth toward the spacecraft mass center lies in the x''–z'' plane. Slew motion is along both the x''- and y''-coordinates. Thus, $\vec{\omega}_s = (\omega_{sx}, \omega_{sy}, 0)$ and $\vec{\alpha}_s = (\alpha_{sx}, \alpha_{sy}, 0)$, $\ddot{\vec{R}}_p$ due to slew motion becomes

$$\ddot{\vec{R}}_{p,\text{slew}} = \begin{bmatrix} \ddot{R}_{x''} \\ \ddot{R}_{y''} \\ \ddot{R}_{z''} \end{bmatrix}_{\text{slew}} = \begin{bmatrix} \omega_{sy}(\omega_{sx}R_y - R_x\omega_{sy}) + \alpha_{sy}R_z + 2\omega_{sy}v_z \\ -\omega_{sx}(\omega_{sx}R_y - R_x\omega_{sy}) - \alpha_{sx}R_z - 2\omega_{sx}v_z \\ -R_z(\omega_{sx}^2 + \omega_{sy}^2) + (\alpha_{sx}R_y - \alpha_{sy}R_x) + 2(\omega_{sx}v_y - \omega_{sy}v_x) \end{bmatrix}_{\text{slew}} \quad \ldots\ldots(3\text{-}10)$$

3.2. Jitter acceleration The sources of residual acceleration of gravity jitter, which range from slew motion of spacecraft, atmospheric drag on the spacecraft, background gravity, spacecraft attitude motions arising from machinery vibrations, thruster firings, crew motion, etc., are also capable for the excitation of slosh waves in spacecraft fluid systems.[1-10]

Among all of the varieties of jitter accelerations listed, accelerations induced by slew motion of the spacecraft dominate the forces activated on the spacecraft fluid systems. Two coordinate systems (cylindrical and cartesian) chosen in this study are (r, θ, z) with corresponding velocity components (u_r, u_θ, u_z) for cylindrical, and (x, y, z) with corresponding velocity components (u_x, u_y, u_z) for cartesian coordinates. The origin of these two coordinates are located at the central bottom of the dewar tank, as shown in Fig. 1. The spacecraft center of mass, is located at $(x_c, y_c, z_c) = (0, 0, L_c)$. The relationships of the force between cartesian and cylindrical coordinates are

$$\begin{bmatrix} \ddot{R}_x \\ \ddot{R}_y \\ \ddot{R}_z \end{bmatrix}_{\text{slew}} = \begin{bmatrix} F_x \\ F_y \\ F_z \end{bmatrix}_{\text{slew}} = \begin{bmatrix} \cos\theta & \sin\theta & 0 \\ -\sin\theta & 0 & 0 \\ 0 & 0 & 1 \end{bmatrix}^{-1} \begin{bmatrix} F_r \\ F_\theta \\ F_z \end{bmatrix}_{\text{slew}} \quad \ldots\ldots(3\text{-}11)$$

A detailed expression of $[\ddot{R}_x, \ddot{R}_y, \ddot{R}_z]_{\text{slew}}$ are shown in Eq. (3-10) of this paper. Jitter acceleration is a summation of acceleration induced by slew motion and others, such as atmospheric drag on the spacecraft, spacecraft attitude motions arising from machinery vibration, thruster firing, crew motion, etc. Thus; jitter acceleration can be expressed as

$$\hat{a}_{gj}=\begin{bmatrix} a_{gj,r} \\ a_{gj,\theta} \\ a_{gj,z} \end{bmatrix}_{slew}+\begin{bmatrix} a_{gj,r} \\ a_{gj,\theta} \\ a_{gj,z} \end{bmatrix}_{others}=-\begin{bmatrix} F_r \\ F_\theta \\ F_z \end{bmatrix}_{slew}-\begin{bmatrix} F_r \\ F_\theta \\ F_z \end{bmatrix}_{others}$$
$$\cdot\left\{1+\frac{1}{2}\sin(2\pi ft)\right\}$$
$$=-\begin{bmatrix} \cos\theta & \sin\theta & 0 \\ -\sin\theta & \cos\theta & 0 \\ 0 & 0 & 1 \end{bmatrix}\begin{bmatrix} F_x \\ F_y \\ F_z \end{bmatrix}_{slew}-\begin{bmatrix} F_r \\ F_\theta \\ F_z \end{bmatrix}_{others}$$
$$\cdot\left\{1+\frac{1}{2}\sin(2\pi ft)\right\} \quad \ldots.(3\text{-}12)$$

where f is the jitter frequency (Hz) imposed on the fluid systems of the spacecraft.

4. Mathematical Model of Sloshing Dynamics Driven by Orbital Acceleration Associated With Spinning and/or Slew Motions

Dynamical behavior of fluid elements inside the on-orbit spacecraft fluid systems are strongly modified by the gravity jitter acceleration associated with slew motion. In order to accommodate the impact of gravity jitter acceleration, in particular, on the on-orbit fluid motion, one has to consider non-inertia frame of the spacecraft bound coordinate rather than adopting inertia frame coordinate used in ordinary fluid mechanics formulation.[25]

Consider a closed circular cylinder of radius, a, with height, L, which is partially filled with cryogenic liquid helium, and the rest of the ullage is filled with a helium vapor. Density and viscosity of liquid helium and helium vapor are ρ_L, μ_L, ρ_v, and μ_v, respectively. Let us use the cylindrical coordinates (r, θ, z), with corresponding velocity components (u, v, w), and corresponding components of gravity jitter acceleration associated with slew motion are $(a_{gj,r}, a_{gj,\theta}, a_{gj,z})$. The typical governing equations of continuity and full Navier-Stokes equations in non-inertia frame cylindrical coordinates are used in this study.[25]

For the purpose of solving sloshing dynamic problems of liquid propellant systems in orbital spacecraft under microgravity environment, one has to solve the governing equations[25] accompanied by a set of initial and boundary conditions. A detailed illustration of these initial and boundary conditions concerning sloshing dynamics of fluid systems in microgravity were precisely given by Hung and Pan.[26] Due to page limitation, the information is not repeated in this paper. Interested readers are suggested to refer to these references.[25,26] Detailed descriptions of the computational algorithm applicable to cryogenic fluid management under microgravity are also given in our earlier studies.[6-10] In this paper, a full-scale AXAF spacecraft propellant dewar tanks with a radius of 68 cm and a height of 145 cm will be used in the numerical simulation. The propellant tank is 70% filled with cryogenic liquid helium for AXAF-S dewar while the rest of the ullage is filled with helium vapor. The temperature of cryogenic helium is 1.3°K. In this study the following data were used: liquid helium density = 145.6 kg/m^3, helium vapor density = 1.47 kg/m^3, fluid pressure = 1.6625 Pa, surface tension coefficient

at the interface between liquid helium and helium vapor = 0.0354 N/m, liquid helium viscosity coefficient = 1.12×10^{-8} m^2/s; and contact angle = 5°. The initial profiles of the liquid-vapor interface for the rotating dewar are determined from computations based on algorithms developed for the steady state formulation of microgravity fluid management.[27]

A staggered grid for the velocity components is used in this computer program. The method was developed by Harlow and Welch[28] for their MAC (marker-and-cell) method of studying fluid flows along a free surface. The finite difference method employed in this numerical study was the "Hybrid Scheme" developed by Spalding.[29] The formulation for this method is valid for any arbitrary interface location between the grid points and is not limited to middle point interfaces.[30] An algorithm for a semi-

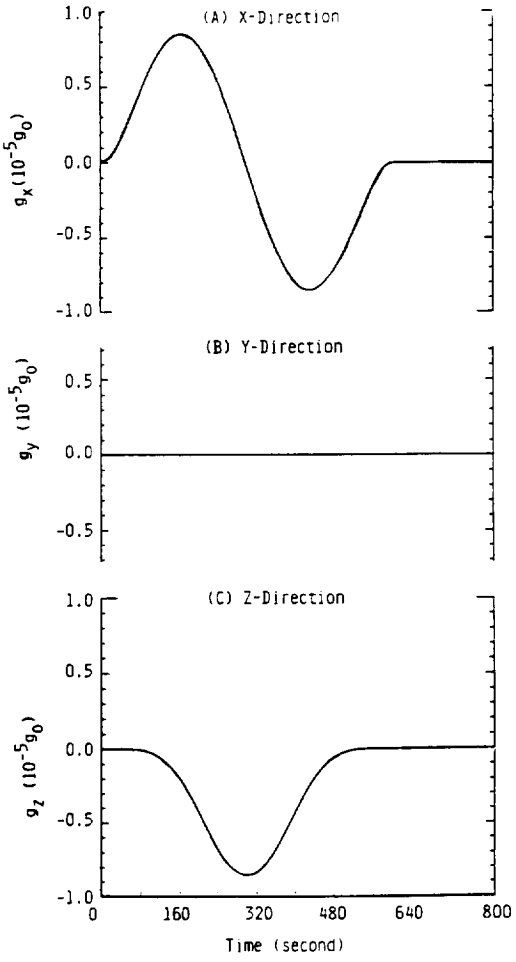

Fig. 2. Time variation of AXAF-S spacecraft jitter acceleration associated with slew motion acting on fluid mass located at $(r, \theta, z) = (12\,\text{cm}, \pi/2, 3\,\text{cm})$ for 90° slew motion in 10 min along the y''-axis and orbital period of 97.6 min. (A) Along x-direction; (B) Along y-direction; (C) Along z-direction.

implicit method[31] was used as the procedure for modeling the flow field. The time step is determined automatically based on the size of the grid points and the velocity of flow fields. A detailed description of the computational algorithm applicable to microgravity fluid management is illustrated in our earlier studies.[6-10] Figures 2(A) and 2(B) show the similar distribution of grid points for the dewar tank for the AXAF-S spacecraft in the radial-axial plane and radial-circumferential plane, respectively, in cylindrical coordinates.

5. Sloshing Dynamics Driven by Jitter Acceleration Associated With Slew Motion

By using the mathematical formulations illustrated in the previous sections, one can numerically simulate spacecraft sloshing dynamics associated with spinning and/or slew motions depending upon the specific scientific missions assigned to the spacecraft. As we indicated earlier, AXAF-S spacecraft is capable to observe point and extended source of active galactic nuclei, clusters of galaxies, supernova remnants, X-ray binaries, etc., through spacecraft slew motion of pointing control.

If slew motion operates with a range of 90° in 10 min (=600 s), the component of

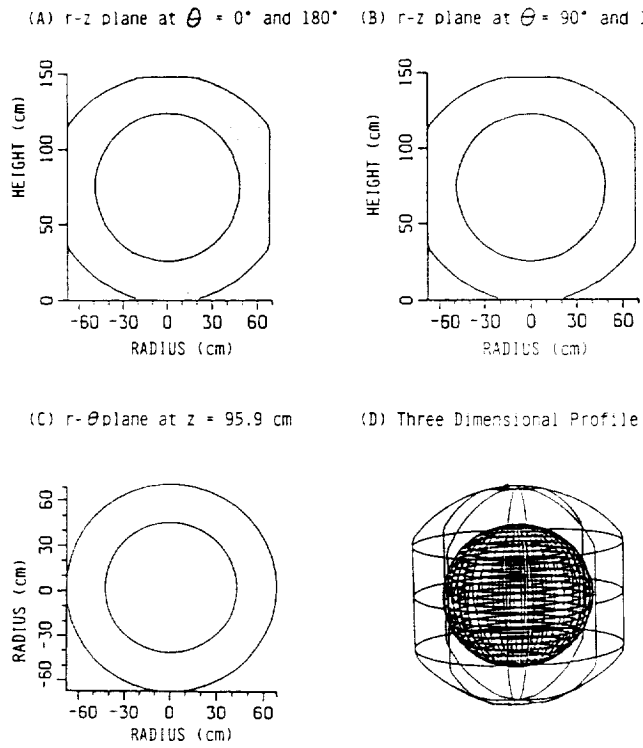

Fig. 3. Initial profiles of liquid-vapor interface for AXAF-S spacecraft of dewar tank under background gravity of $10^{-7} g_0$ and direction of background gravity at $\psi_E = 0°$. (A) In r–z plane at $\theta = 0°$ and 180°, (B) In r–θ plane at $\theta = 90°$ and 270°, (C) In r–θ plane at $z = 95.9$ cm, and (D) Three-dimensional liquid-vapor interface profile.

jitter acceleration, based on Eqs. (3-9) to (3-12), along the (x, y, z) directions acted on the fluid mass located at $(r, \theta, z) = (12\,\text{cm}, \pi/2, 3\,\text{cm})$ is shown in Fig. 2. This figure shows that the magnitude of gravity gradient acceleration is on the order of $10^{-5} g_0$.

The equilibrium shape of the liquid-vapor interface for a dewar with 70% liquid-filled level under a residual gravity environment below $10^{-6} g_0$ is a sphere. Figure 3(A) shows the initial shape of the interface in the r–z plane at $\theta = 0°$ and 180°; Fig. 3(B) shows the initial profile of the liquid-vapor interface in the r–z plane at $\theta = 90°$ and 270°; Fig. 3(C) shows the initial profile of the liquid-vapor interface in the r–θ plane at height $z = 95.9\,\text{cm}$; and Fig. 3(D) shows the initial profile of three-dimensional liquid-vapor interface. Because of page limitation, time evolution of liquid-vapor

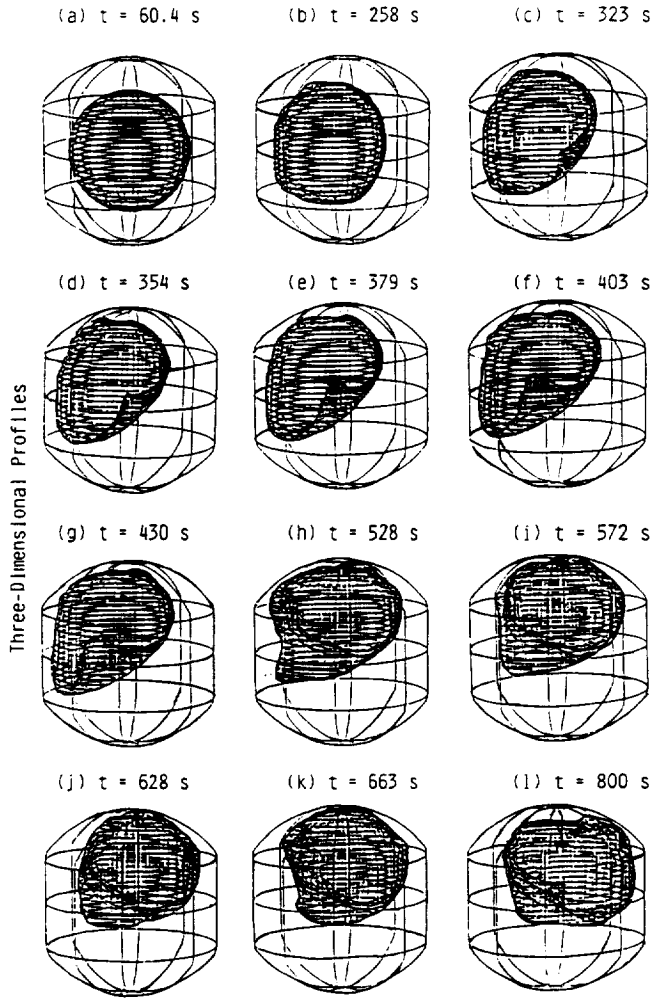

Fig. 4. Time sequence evolution of AXAF-S spacecraft three-dimensional liquid-vapor interface oscillations for dewar driven by jitter acceleration associated with slew motion in the y''-axis. 90° slew motion in 10 min is applied to the spacecraft operation.

interface profiles for initial shapes shown in Figs. 3(A) and 3(D) only will be illustrated.

Figure 4 shows the time sequence evolution of the three-dimensional behavior of the interface oscillations driven by jitter acceleration associated with slew motion. It is shown in this figure that a time sequence evolution of liquid-vapor interface profiles at time $t=60.4$, 258, 323, 354, 379, 403, 430, 528, 572, 628, 663, and 800 s are illustrated. It clearly shows that there are a series of asymmetric oscillations excited along the surface of sloshing dynamics governed liquid-vapor interface driven by asymmetric jitter acceleration associated with slew motion.

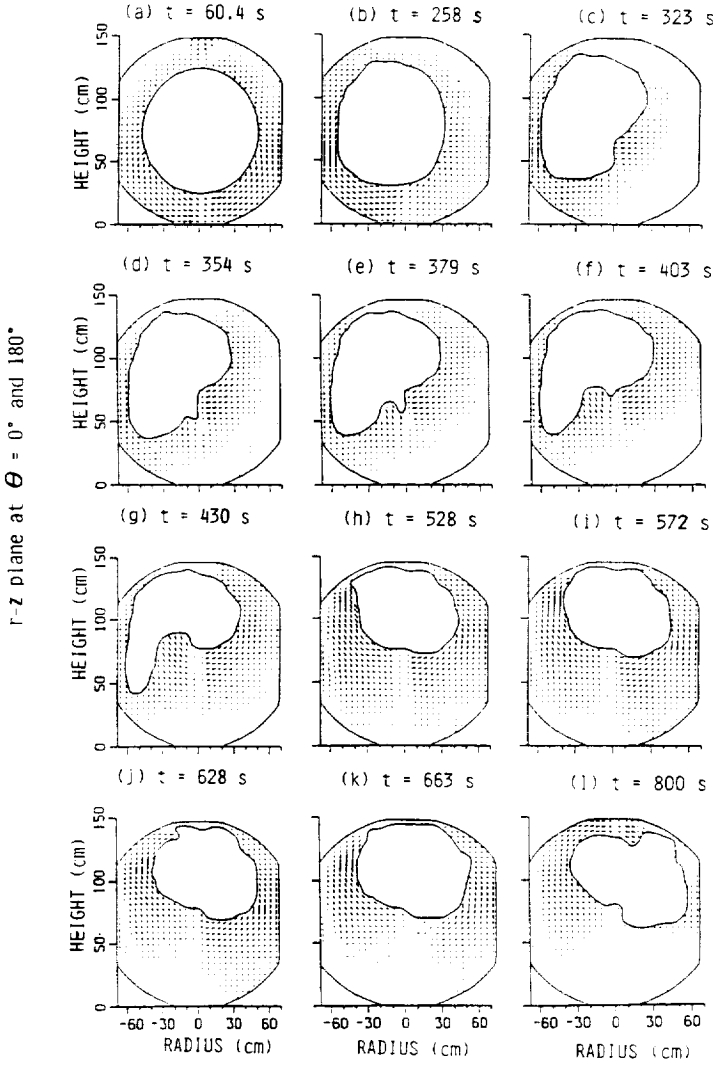

Fig. 5. Time sequence evolution of AXAF-S spacecraft liquid-vapor interface oscillations for dewar tank in r–z plane at $\theta=0°$ and 180°, driven by jitter acceleration associated with slew motion in the y''-axis. 90° slew motion in 10 min is applied to the spacecraft operation.

Figure 5 shows the time sequence of the sloshing dynamics governed liquid-vapor interface profiles, driven by the same jitter acceleration associated with slew motion as that shown in Fig. 4, in the vertical r–z plane at $\theta=0°$ and 180°. It clearly indicates that the spherical shape bubble (helium vapor) configurations change from axial symmetric to asymmetric profiles during the course of slew motion.

Figure 2 shows that gravity jitter acceleration associated with slew motion is pointing toward the southeastern direction at the very beginning and then is pointing toward the southwestern direction at the end in the x–z plane (or r–z plane at $\theta=0°$ and 180°). These indicate that liquid is pushed toward the southeastern and then toward the southwestern directions (the bubble is pushed toward the northwestern and then toward the northeastern directions) in r–z plane at $\theta=0°$ and 180°. Figures 4 and 5 exactly demonstrate these results.

6. Characteristics of Sloshing Dynamics Induced Fluctuations in Fluid System Moment and Angular Momentum

Sloshing dynamics induced fluctuations in the fluid system of spacecraft dewar tank introduce time-dependent disturbances in moment and angular momentum of spacecraft fluid system. In this study, there are induced angular velocities along the yawing, pitching and rolling axes due to the fluid motion inside the dewar container. These angular velocities in yawing, pitching and rolling axes, caused by the fluid flows in a partially liquid-filled container, readjust the angular velocity in the dewar container.

In order to accommodate the spacecraft dynamics of yawing, pitching and rolling, cylindrical coordinates of dewar container is transformed into cartesian coordinates based on $(x, y, z)=(r\cos\theta, r\sin\theta, z)$ with corresponding velocity components $(V_x, V_y, V_z)=(u\cos\theta-v\sin\theta, u\sin\theta+v\cos\theta, w)$. If spacecraft is rotated with respect to mass center at (r_c, θ_c, z_c) in cylindrical coordinates, location of mass center in cartesian coordinates becomes $(x_c, y_c, z_c)=(r_c\cos\theta_c, r_c\sin\theta_c, z_c)$. Induced angular velocities $(\tilde{\omega}_x, \tilde{\omega}_y, \tilde{\omega}_z)$ in cartesian coordinates becomes

$$\begin{bmatrix} \tilde{\omega}_x \\ \tilde{\omega}_y \\ \tilde{\omega}_z \end{bmatrix} = \begin{bmatrix} K_{xx} & -K_{xy} & K_{xz} \\ K_{yx} & K_{yy} & -K_{yz} \\ -K_{zx} & K_{zy} & K_{zz} \end{bmatrix} \begin{bmatrix} V_x \\ V_y \\ V_z \end{bmatrix} \quad \ldots\ldots(6\text{-}1)$$

where

$$K_{xx}=K_{yy}=K_{zz}=0$$

$$\begin{bmatrix} K_{xy} \\ K_{yx} \end{bmatrix} = (z-z_c) \begin{bmatrix} [(y-y_c)^2+(z-z_c)^2]^{-1} \\ [(x-x_c)^2+(z-z_c)^2]^{-1} \end{bmatrix}$$

$$\begin{bmatrix} K_{xz} \\ K_{zx} \end{bmatrix} = (y-y_c) \begin{bmatrix} [(y-y_c)^2+(z-z_c)^2]^{-1} \\ [(x-x_c)^2+(y-y_c)^2]^{-1} \end{bmatrix}$$

$$\begin{bmatrix} K_{yz} \\ K_{zy} \end{bmatrix} = (x-x_c) \begin{bmatrix} [(x-x_c)^2+(z-z_c)^2]^{-1} \\ [(x-x_c)^2+(y-y_c)^2]^{-1} \end{bmatrix}$$

As the velocity components are given by

$$\begin{bmatrix} V_x \\ V_y \\ V_z \end{bmatrix} = \begin{bmatrix} \cos\theta & -\sin\theta & 0 \\ \sin\theta & \cos\theta & 0 \\ 0 & 0 & 1 \end{bmatrix} \begin{bmatrix} u \\ v \\ w \end{bmatrix}, \qquad \ldots\ldots(6\text{-}2)$$

the relationship between the components of induced angular velocity and flow velocity in cylindrical coordinates can be expressed in the following formulation:

$$\begin{bmatrix} \tilde{\omega}_x \\ \tilde{\omega}_y \\ \tilde{\omega}_z \end{bmatrix} = \begin{bmatrix} \tilde{K}_{xx} & \tilde{K}_{xy} & \tilde{K}_{xz} \\ \tilde{K}_{yx} & \tilde{K}_{yy} & \tilde{K}_{yz} \\ \tilde{K}_{zx} & \tilde{K}_{zy} & \tilde{K}_{zz} \end{bmatrix} \begin{bmatrix} u \\ v \\ w \end{bmatrix} \qquad \ldots\ldots(6\text{-}3)$$

where

$$\begin{bmatrix} \tilde{K}_{xx} \\ \tilde{K}_{xy} \\ \tilde{K}_{xz} \end{bmatrix} = \begin{bmatrix} -(z-z_c)\sin\theta \\ -(z-z_c)\cos\theta \\ r\sin\theta - r_c\sin\theta_c \end{bmatrix} [(r\sin\theta - r_c\sin\theta_c)^2 + (z-z_c)^2]^{-1}$$

$$\begin{bmatrix} \tilde{K}_{yx} \\ \tilde{K}_{yy} \\ \tilde{K}_{yz} \end{bmatrix} = \begin{bmatrix} (z-z_c)\cos\theta \\ -(z-z_c)\sin\theta \\ -(r\cos\theta - r_c\cos\theta_c) \end{bmatrix} [(r\cos\theta - r_c\cos\theta_c)^2 + (z-z_c)^2]^{-1}$$

$$\begin{bmatrix} \tilde{K}_{zx} \\ \tilde{K}_{zy} \\ \tilde{K}_{zz} \end{bmatrix} = \begin{bmatrix} -r_c\sin(\theta-\theta_c) \\ r - r_c\cos(\theta-\theta_c) \\ 0 \end{bmatrix} [r^2 + r_c{}^2 - 2rr_c\cos(\theta-\theta_c)]^{-1}$$

For the case of the AXAF-S Spacecraft, axis of slew motion is always fixed at the point of spacecraft mass center which is located at (0, 0, L_c), where L_c is the height of the axis of slew motion (see Fig. 1). By using the computed results of induced angular velocity shown in Eq. (6-3), one can compute the angular momentum (H_x, H_y, H_z) as follows:

$$\begin{bmatrix} H_x \\ H_y \\ H_z \end{bmatrix} = \rho_v \iiint \begin{bmatrix} \tilde{I}_{xx} & -\tilde{I}_{xy} & -\tilde{I}_{xz} \\ -\tilde{I}_{yx} & \tilde{I}_{yy} & -\tilde{I}_{yz} \\ -\tilde{I}_{zx} & -\tilde{I}_{zy} & \tilde{I}_{zz} \end{bmatrix} \begin{bmatrix} \tilde{\omega}_x \\ \tilde{\omega}_y \\ \tilde{\omega}_z \end{bmatrix} r\,d\theta\,dr\,dz$$

$$+ \rho_L \iiint \begin{bmatrix} \tilde{I}_{xx} & -\tilde{I}_{xy} & -\tilde{I}_{xz} \\ -\tilde{I}_{yx} & \tilde{I}_{yy} & -\tilde{I}_{yz} \\ -\tilde{I}_{zx} & -\tilde{I}_{zy} & \tilde{I}_{zz} \end{bmatrix} \begin{bmatrix} \tilde{\omega}_x \\ \tilde{\omega}_y \\ \tilde{\omega}_z \end{bmatrix} r\,d\theta\,dr\,dz \qquad \ldots\ldots(6\text{-}4)$$

where

$$\tilde{I}_{xx} = r^2\sin^2\theta + (z-L_c)^2 \;;\quad \tilde{I}_{xy} = \tilde{I}_{yx} = r^2\sin\theta\cos\theta$$
$$\tilde{I}_{yy} = r^2\cos^2\theta + (z-L_c)^2 \;;\quad \tilde{I}_{xz} = \tilde{I}_{zx} = r(z-L_c)\cos\theta$$
$$\tilde{I}_{zz} = r^2 \qquad\qquad\quad ;\quad \tilde{I}_{yz} = \tilde{I}_{zy} = r(z-L_c)\sin\theta$$

The moment of spacecraft can be computed from the time rate of change of the angular momentum, i.e.,

$$\begin{bmatrix} M_x \\ M_y \\ M_z \end{bmatrix} = \frac{d}{dt}\begin{bmatrix} H_x \\ H_y \\ H_z \end{bmatrix} + \begin{bmatrix} \omega_y H_z & -\omega_z H_y \\ \omega_z H_x & -\omega_x H_z \\ \omega_x H_y & -\omega_y H_x \end{bmatrix} \quad \ldots\ldots(6\text{-}5)$$

where $\omega_i = (\omega_x, \omega_y, \omega_z)$ denotes pitching, yawing and rolling angular velocities of spacecraft in inertia frame.

7. Sloshing Dynamics Induced Angular Momentum and Moment Fluctuations Driven by Gravity Jitter Acceleration Associated With Slew Motion

Figures 6(A), 6(B) and 6(C) show the computed time variation of the fluctuations of angular momentum driven by gravity jitter acceleration associated with slew motion along the x, y and z axes, respectively. This figure shows the following results: (a) The values of angular momentum fluctuations are $(\Delta H_x, \Delta H_y, \Delta H_z) = (0.4, 17.55, 0.161)$ $10^6\,\mathrm{g\cdot cm^2/s}$, it clearly indicates $\Delta H_y > \Delta H_x > \Delta H_z$. The maximum absolute values of angular moment are Max $(|H_x|, |H_y|, |H_z|) = (0.275, 8.92, 0.091)$ $10^6\,\mathrm{g\cdot cm^2/s}$. It also indicates $|H_y| > |H_x| > |H_z|$. (b) The initial values of H_x, H_y and H_z start from zero value in non-inertia frame. (c) Variations of H_y dominates the whole spectrum of angular momentum fluctuations because angular displacement in the y-axis is the only slew motion in the entire process, while the variations of H_x and H_z are much smaller than H_y because there is no slew motion applied on the x- and z-axes.

Figures 7(A), 7(B) and 7(C) show variations of fluid moments due to sloshing dynamics driven by gravity jitter acceleration associated with slew motion along the x, y and z axes, respectively. The values of fluid moment fluctuations are $(\Delta M_x, \Delta M_y, \Delta M_z) = (13.38, 200.79, 4.32)$ $10^3\,\mathrm{dyn\cdot cm}$. The maximum absolute values of fluid moment are Max $(|M_x|, |M_y|, |M_z|) = (6.77, 100.75, 2.33)$ $10^3\,\mathrm{dyn\cdot cm}$. It shows $\Delta M_y > \Delta M_x > \Delta M_z$ and $|M_y| > |M_x| > |M_z|$. Characteristics of the fluctuations of fluid moments due to sloshing dynamics driven by gravity jitter acceleration associated with slew motion in the y-axis draw three point conclusions similar to that drawn for the fluctuations of angular momentum of fluid system.

8. Discussion and Conclusion

With different scientific missions, some experimental spacecrafts have to operate with various kinds of slew motion for the purpose to perform its scientific experiments. In this study, the AXAF-S spacecraft has been given as an example to show a spacecraft operated with slew motion. The instability of the liquid-vapor interface surface of the fluid systems can be induced by the presence of gravity jitter acceleration associated with slew motion of the spacecraft.[32] These instabilities originated from sloshing dynamics can cause various problems of spacecraft control systems.[8] Sometimes, these sloshing dynamics problems can even deteriorate the quality of the normal operation of the spacecraft. It is vitally important to understand fully the characteristics of the spacecraft sloshing dynamics before one can assure the high quality operation of scientific spacecraft.[8]

In this paper, the mathematical formulation of sloshing dynamics and associated fluctuations of fluid moment and angular momentum for partially filled liquid in the

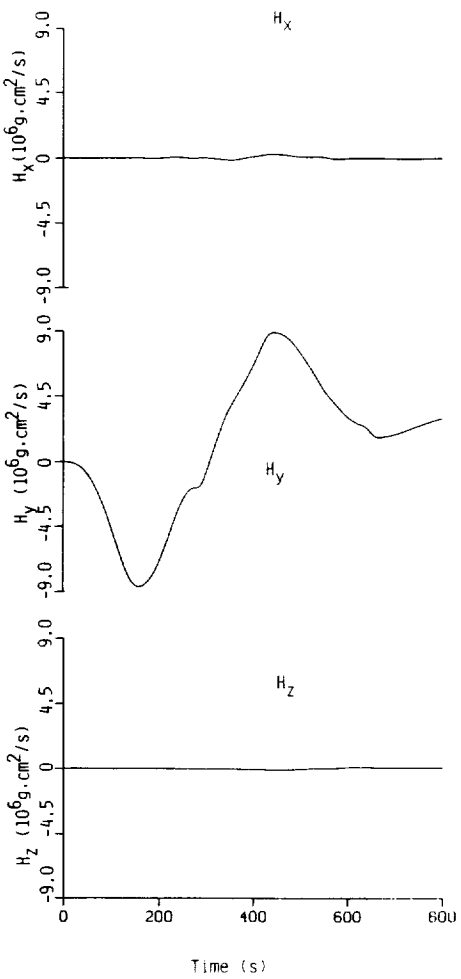

Fig. 6. Time sequence of the AXAF-S spacecraft angular momentum fluctuations (H_x, H_y, H_z) due to the sloshing dynamics driven by gravity jitter acceleration associated with slew motion in the y-axis. 90° slew motion in 10 min is applied to spacecraft operation.

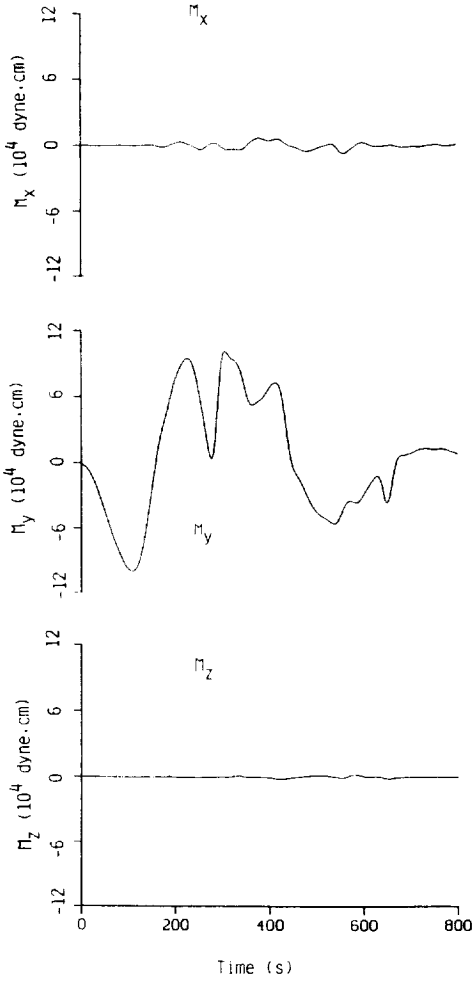

Fig. 7. Time sequences of the AXAF-S spacecraft fluid moment fluctuations due to sloshing dynamics driven by gravity jitter acceleration associated with slew motion in the y-axis. 90° slew motion in 10 min is applied to spacecraft motion. (A) For moment along x-direction; (B) For moment along y-direction; and (C) For moment along z-direction.

dewar container driven by the gravity jitter acceleration associated with slew motion are investigated.

The numerical simulation of fluid moment and angular momentum fluctuations due to sloshing dynamics driven by gravity jitter acceleration associated with slew motion, with AXAF-S as an example, have been carried out. Results show that there are a large amplitude fluctuations of angular momentum along the y-axis which reflects

the characteristics and the trend of slew motion in the y-axis. The example demonstrates how great the degrees of sloshing dynamics affected fluid moment and angular momentum fluctuations and their relationship to the major driving force of gravity jitter acceleration associated with slew motion. The mathematical formulations shown in this study can provide a better understanding of how fluid flows affected by orbital acceleration in a dewar container, and also provide a useful tool for the development of effective control techniques to assure the high quality operation of the spacecraft to achieve the final goal of scientific missions.[8]

Acknowledgement

The authors appreciate the support received from the National Aeronautics and Space Administration through the NASA Grant NAG8-938, and also NASA contracts NAS8-38609/Delivery Order No. 96 and Delivery Order No. 103. They would like to express their gratitude to Richard A. Potter of NASA/Marshall Space Flight Center for the stimulating discussions during the course of the present study.

References

1) Kamotani, Y., Prasad, A. and Ostrach, S.: Thermal Convection in an Enclosure Due to Vibration Abroad a Spacecraft, *AIAA J.*, **19** (1981), pp. 511–516.
2) Hung, R. J. and Shyu, K. L.: Cryogenic Liquid Hydrogen Reorientation Activated by High Frequency Impulsive Reverse Gravity Acceleration of Geyser Initiation, *Microgravity Q.*, **1**(2) (1991), pp. 81–92.
3) Hung, R. J. and Shyu, K. L.: Space-Based Cryogenic Liquid Hydrogen Reorientation Activated by Low Frequency Impulsive Reverse Gravity Thruster of Geyser Initiation, *Acta Astronautica*, **25** (1991), pp. 709–719.
4) Hung, R. J. and Shyu, K. L.: Constant Reverse Thrust Activated Reorientation of Liquid Hydrogen with Geyser Initiation, *J. Spacecraft and Rockets*, **29** (1992), pp. 279–285.
5) Hung, R. J. and Shyu, K. L.: Excitation of Slosh Waves Associated with Low Frequency Impulsive Reverse Gravity Acceleration of Geyser Initiation, *Acta Astronautica*, **26** (1992), pp. 425–433.
6) Hung, R. J. and Shyu, K. L.: Medium Frequency Impulsive Thrust Activated Liquid Hydrogen Reorientation with Geyser, *J. Propulsion and Power*, **8** (1992), pp. 987–994.
7) Hung, R. J., Lee, C. C. and Leslie, F. W.: Response of Gravity Level Fluctuations on the Gravity Probe-B Spacecraft Propellant System, *J. Propulsion and Power*, **7** (1991), pp. 556–564.
8) Hung, R. J., Lee, C. C. and Leslie, F. W.: Spacecraft Dynamical Distribution of Fluid Stresses Activated by Gravity Jitter Induced Slosh Waves, *J. Guidance, Control and Dynamics*, **15** (1992), pp. 817–824.
9) Hung, R. J., Lee, C. C. and Leslie, F. W.: Similarity Rules in Gravity Jitter-Related Spacecraft Liquid Propellant Slosh Waves Excitation, *J. Fluids and Structures*, **6** (1992), pp. 493–522.
10) Hung, R. J., Lee, C. C. and Leslie, F. W.: Effect of the Baffle on the Spacecraft Fluid Propellant Viscous Stress and Moment Fluctuations, *Trans. Japan Soc. Aeronaut. Space Sci.*, **35** (1993), pp. 187–207.
11) Hung, R. J., Tsao, Y. D., Hong, B. B. and Leslie, F. W.: Dynamical Behavior of Surface Tension on Rotating Fluids in Low and Microgravity Environments, *Int. J. Microgravity Res. Appl.*, **11** (1989), pp. 81–95.

12) Hung, R. J., Tsao, Y. D., Hong, B. B. and Leslie, F. W.: Axisymmetric Bubble Profiles in a Slowly Rotating Helium Dewar Under Low and Microgravity Environments, *Acta Astronautica*, **19** (1989), pp. 411–426.
13) Hung, R. J., Tsao, Y. D., Hong, B. B. and Leslie, F. W.: Bubble Behaviors in a Slowly Rotating Helium Dewar in Gravity Probe-B Spacecraft Experiment, *J. Spacecraft and Rockets*, **26** (1989), pp. 167–172.
14) Leslie, F. W.: Measurements of Rotating Bubble Shapes in a Low Gravity Environment, *J. Fluid Mech.*, **161** (1985), pp. 269–275.
15) Mason, P., Collins, D., Petrac, D., Yang, L., Edeskuty, F., Schuch, A. and Williamson, K.: The Behavior of Superfluid Helium in Zero Gravity, *Proceedings 7th International Cryogenic Engineering Conferences*, Science and Technology Press, Surrey, England, 1978.
16) Avduyevsky, V. S. (Ed.): *Scientific Foundations of Space Manufacturing*, MIR, Moscow, USSR, 1984.
17) Forward, R. L.: Flattening Space-Time Near the Earth, *Phys. Rev., Series D*, **26** (1982), pp. 735–744.
18) Misner, C. W., Thorne, K. S. and Wheeler, J. A.: *Gravitation*, W. H. Freeman Co., San Francisco, CA, 1973, pp. 1–1279.
19) Van Sciver, S. W.: *Helium Cryogenics*, Plenum Press, New York, 1986, p. 429.
20) Donnelly, R. J.: *Quantized Vortices in Helium II*, Cambridge University Press, Cambridge, 1991, p. 346.
21) Wilks, J.: *The Properties of Liquid and Solid Helium*, Clarendon Press, Oxford, U.K., 1967.
22) Hoare, F. E., Jackson, L. C. and Kurti, N.: *Experimental Cryogenics; Liquid Helium II*, Butterworths, London, U.K., 1961.
23) Hung, R. J.: Superfluid and Normal Fluid Helium II in a Rotating Tank Under Low and Microgravity Environments, *Proc. Natl. Sci. Council, Series (A)*, **14** (1990), pp. 289–290.
24) Hung, R. J. and Lee, C. C.: Characteristics and Behaviors of Gravity Probe-B Spacecraft Propulsion System, *Proc. Natl. Sci. Council (A)*, **16** (1992), pp. 339–352.
25) Hung, R. J., Pan, H. L. and Leslie, F. W.: Gravity Gradient or Gravity Jitter Induced Viscous Stress and Moment Fluctuations in Microgravity, *Fluid Dynamics Res.*, **14** (1994), pp. 29–51.
26) Hung, R. J. and Pan, H. L.: Asymmetric Slosh Wave Excitation in Liquid-Vapor Interface Under Microgravity, *Acta Mech. Sinica*, **9** (1993), pp. 298–311.
27) Hung, R. J. and Leslie, E. W.: Bubble Shapes in a Liquid-Filled Rotating Container Under Low Gravity, *J. Spacecraft and Rockets*, **25** (1988), pp. 70–74.
28) Harlow, F. H. and Welch, F. E.: Numerical Calculation of Time-Dependent Viscous Incompressible Flow of Fluid With Free Surface, *Phys. of Fluids*, **8** (1965), pp. 2182–2189.
29) Spalding, D. B.: A Novel Finite-Difference Formulation for Differential Expressions Involving Both First and Second Derivatives, *Int. J. Numer. Meth. Engin.*, **4** (1972), pp. 551–559.
30) Patanker, S. V. and Spalding, S. D.: A Calculation Procedure for Heat, Mass and Momentum Transfer in Three Dimensional Parabolic Flows, *Int. J. Heat Mass Transfer*, **15** (1972), pp. 1787–1805.
31) Patanker, S. V.: *Numerical Heat Transfer and Fluid Flow*, Hemisphere-McGraw-Hill, New York, NY, 1980, p. 197.
32) Hung, R. J. and Pan, H. L.: Difference in Gravity Gradient and Gravity Jitter-Excited Slosh Waves in Microgravity, *Trans. Japan Soc. Aeronaut. Space Sci.*, **36** (1993), pp. 153–169.